HVEM Tomography of the *Trans*-Golgi Network: Structural Insights and Identification of a Lace-like Vesicle Coat

Mark S. Ladinsky, James R. Kremer, Paul S. Furcinitti, J. Richard McIntosh, and Kathryn E. Howell*

Laboratory for 3-D Fine Structure, Department of Molecular, Cellular, and Developmental Biology, University of Colorado, Boulder, Colorado 80309-0347; and *Department of Cellular and Structural Biology, University of Colorado Medical School, Denver, Colorado 80262

Abstract. High voltage electron microscopy and computer axial tomography have been used to study the 3-D structure of *trans*-Golgi cisternae and *trans*-Golgi networks (TGNs) in NRK cells. Both structures were specifically labeled by photoconversion of a fluorescent analogue of ceramide using a modification of the technique of Pagano et al. (*J. Cell Biol.* 1991. 113: 1267–1279). Regions of the Golgi ribbon in fixed, stained cells were cut in 250-nm sections and analyzed by tilt series microscopy and subsequent tomographic reconstruction. Resolution of the reconstructions ranged from 6 to 10 nm. The size and structure of the TGN varied considerably throughout the Golgi ribbon; all reconstructions were made from regions with pronounced TGN. Most regions analyzed contained multiple (2–4) Golgi cisternae that stain with ceramide. These "peel off" from the closely stacked cisternae and are continuous at their ends with tubules that contribute to the TGN. Most vesicular profiles visualized in the TGN are connected to TGN tubules. The budding of vesicles appears to occur synchronously along the length of a TGN tubule. Two distinct coats were visualized on budding vesicles: clathrin cages and a novel, lace-like structure. Individual TGN tubules produce vesicles of only one coat type. These observations lead to the following predictions: (*a*) sorting of molecules must occur prior to the formation of TGN tubules; (*b*) vesicle formation takes place almost synchronously along a given TGN tubule; and (*c*) lace-like coats form on exocytic vesicles.

THE Golgi complex is the central organelle in the secretory pathway of all eukaryotic cells (for reviews, Farquhar and Palade, 1981; Rothman and Orci, 1992; and Hong and Tang, 1993). The membranes of the Golgi complex contain enzymes that modify newly synthesized proteins and lipids as well as factors that are involved in sorting these molecules into vesicles for delivery to post-Golgi locations.

Our understanding of the three-dimensional (3-D)[1] structure of the Golgi complex comes mainly from the work of Rambourg and colleagues (Rambourg et al., 1979; Rambourg and Clermont, 1990). In these studies Golgi structure was deduced from stereoscopic images of thick sections taken by both conventional and high voltage electron microscopy. Various staining techniques were employed to label different Golgi regions: hyper-osmication for the *cis* region, and phosphatase cytochemistry for the *medial* (nicotinamideadenyl-diphosphatase) and *trans* regions (thiamine pyrophosphatase [TPPase] or cytidine monophosphatase [CMPase]). Low magnification reconstructions from these preparations has demonstrated that the Golgi complex is a continuous, ribbon-like structure, rather than randomly situated stacks of cisternae, as it appears in conventional thin-section images. This ribbon consisted of aligned cisternal regions, the compact zones, separated by fenestrated regions, the noncompact zones. At higher magnification, the *cis* element was seen to be continuous between adjacent zones and structurally distinguishable from the *medial* and *trans* cisternae. The *cis* elements were composed of a network of anastamosing tubules with no cisternal component. The *medial* and *trans* elements maintained a regular cisternal structure in the compact zones, and became tubular in the noncompact zones.

Rambourg found that the *trans*-Golgi region was composed of 3–5 cisternae that eventually lost register with the preceding elements, "peeling off" from the cisternae in the compact zone. Where these elements lost alignment with the cisternae, they began to anastomose into tubulovesicular networks, forming what was initially referred to as the *trans*-tubular network (Rambourg et al., 1979), but has since become known as the *trans*-Golgi reticulum (Roth et al., 1985) or TGN (Griffiths and Simons, 1986).

Address all correspondence to Mark S. Ladinsky, Laboratory for 3-D Fine Structure, Dept. of Molecular, Cellular, and Developmental Biology, University of Colorado, Boulder, CO 80309-0347. Tel.: (303) 492-7980. Fax: (303) 492-7744.

1. *Abbreviations used in this paper*: 3-D, three dimensional; HMEM, Hepes-supplemented Minimum Essential Medium; HVEM, high voltage electron microscopy; NRK, normal rat kidney; TPPase, thiamine pyrophosphatase.

Rambourg's studies have provided a clear definition of the Golgi "ribbon" and insights into the structure and organization of the Golgi cisternae. However, these studies did not define the TGN as clearly as they did the cisternae for several reasons: first, the 3-D structure of the TGN is far less regular than that of the cisternae, and it varies significantly throughout the ribbon. Rambourg appreciated this by noting the absence of TGN from some regions of his reconstructions (Rambourg et al., 1979). Any single reconstruction or model is insufficient to describe the wide structural variance of the TGN. Second, the resolution of stereo reconstructions, which we estimate to be ~60 nm, is simply not high enough to model adequately the highly complex structure of this region. Third, the specific labeling techniques used by Rambourg did not label all membranes of the TGN. This was shown by comparison of immunogold localization of sialyltransferase on Lowicryl sections with the phosphatase cytochemistry used by Rambourg (Roth et al., 1985). The TPPase and CMPase reactions labeled fewer membranes than sialyltransferase, so Rambourg's reconstructions are unlikely to have identified all components of the TGN.

To effectively study the complex structure of the TGN and adjacent areas, an efficient, specific label is required. The photoconversion of a fluorescently derivatized lipid has solved this problem: ceramide, derivatized with a fluorophore (BODIPY) is taken into cells and partitioned into cellular membranes at 4°C (Pagano et al., 1989, 1991). Upon warming to 37°C, the cells convert the BODIPY-ceramide to BODIPY-sphingomyelin with Golgi enzymes and both BODIPY-ceramide and its metabolites accumulate in the *trans*-Golgi without degradation or liberation of the fluorophore. This provides a specific label for *trans* cisternae, TGN, and later compartments of the secretory pathway. Double-labeling experiments have shown that compartments which label with BODIPY-ceramide are positive for TPPase, indicating that the labeled compartments are *trans*-Golgi or TGN (Pagano et al., 1991). This probe is widely accepted as a label for *trans*-Golgi and as a tool for studying aspects of traffic between the Golgi and plasma membrane (see Cooper et al., 1990; Mellman and Simons, 1992; Takazawa et al., 1993). Once the probe has accumulated in the *trans*-Golgi, the fluorophore can be photobleached by laser irradiation in the presence of diaminobenzidine, resulting in its conversion to an electron-opaque product that is readily visible by thin-section electron microscopy. We have modified this technique to make it suitable for the study of thick sections by high voltage electron microscopy (HVEM) and subsequent 3-D analysis. These methods provide new insights into the 3-D structure of the *trans*-Golgi cisternae and TGN in normal rat kidney (NRK) cells. The potential of these methods for addressing dynamic issues of structure-function relationships within the Golgi is discussed.

Materials and Methods

Cell Culture and BODIPY-ceramide Preparation

NRK cells were cultured in Dulbecco's Modified Eagle's Medium supplemented with 8% FCS in a 37°C, 5% CO_2 humidified atmosphere. BODIPY-ceramide was complexed with BSA as follows: 200 μg C_5-BODIPY-ceramide (D-3521; Molecular Probes, Inc., Eugene, OR) was dissolved in 200 μl EtOH. This solution was added to 10 ml Hepes-supplemented Minimum Essential Medium (HMEM) containing 0.34 mg defatted BSA (A-6003; Sigma Chem. Co., St. Louis, MO)/ml with rapid stirring, and dialyzed overnight against 500 ml of HMEM. The BODIPY-ceramide/BSA complex was recovered and stored at −20°C in 1-ml aliquots.

Cells internalized the ceramide probe according to the procedure of Pagano et al. (1991). Cells were plated onto no. 1 thickness glass coverslips in 30-mm plastic petri dishes and grown to ~90% confluency. The dishes

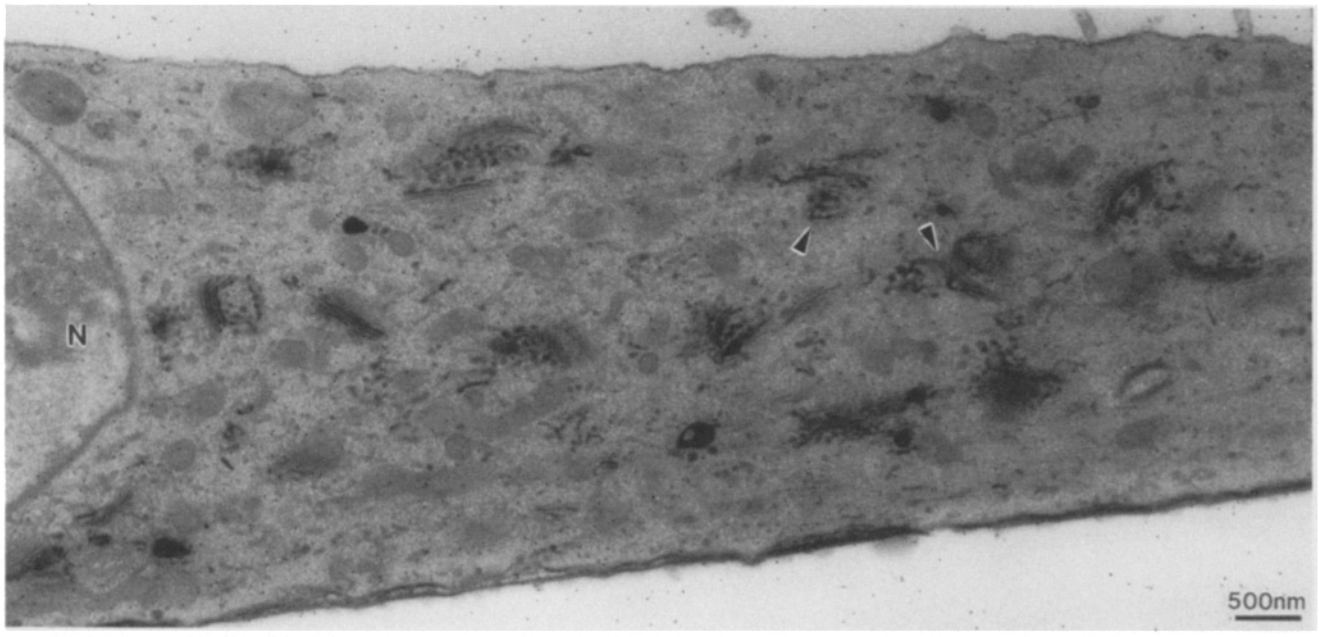

Figure 1. HVEM image of an NRK cell showing the Golgi region. Low magnification images like this were taken prior to beginning a tilt-series to determine the quality of preservation and to identify good areas for analysis. The region contains multiple Golgi stacks, which together form the Golgi ribbon. Two areas (*arrowheads*) were chosen for subsequent tomographic analysis. *N*, nucleus. Bar, 500 nm.

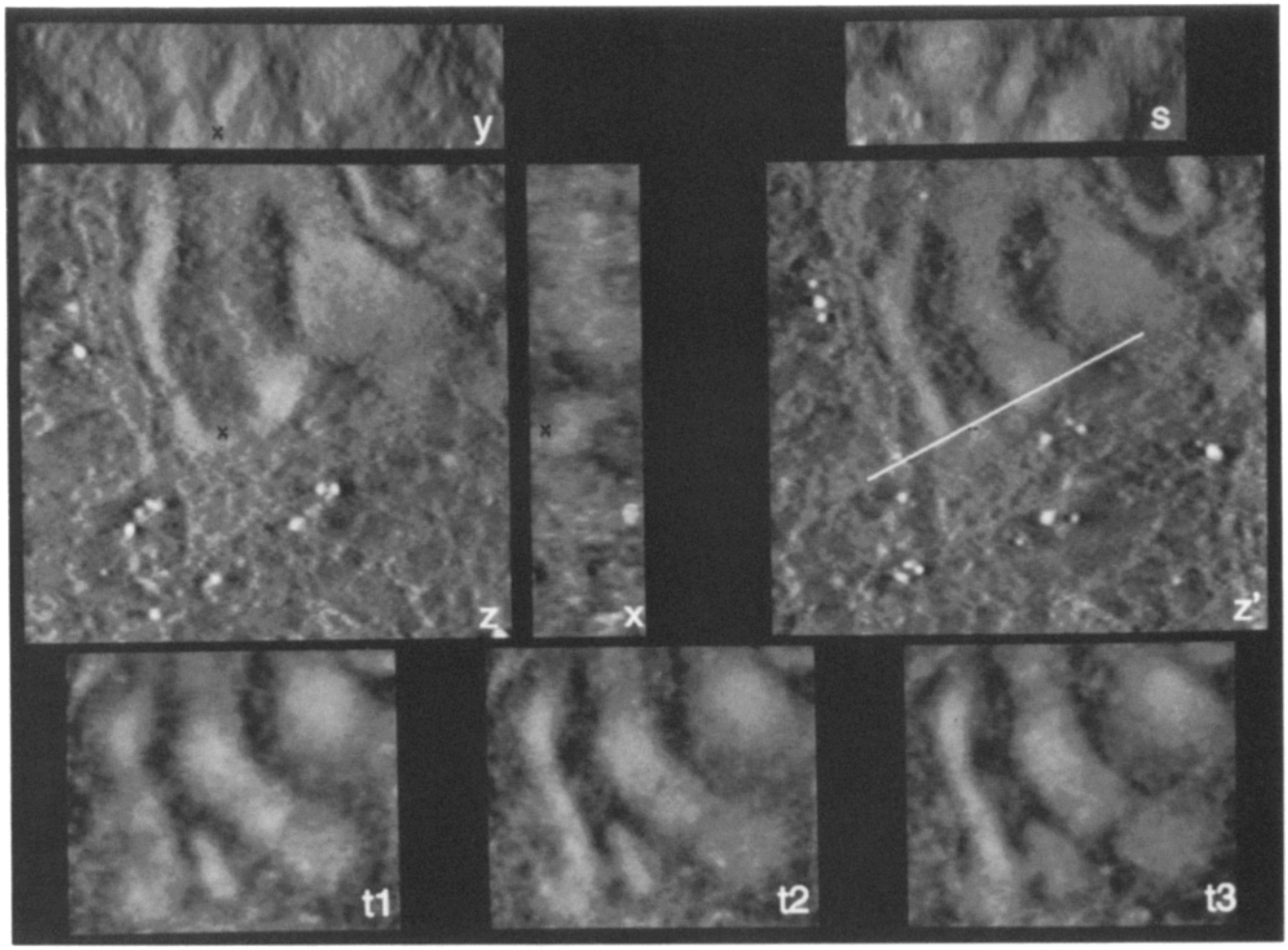

Figure 2. Computer tools used for accurate modeling of tomograms. A region selected from the tomogram shown in Fig. 4 is used to depict the ways problems of membrane continuity were solved using tools available in the IMOD modeling program. *z* is a sub-region of a single 2.4-nm slice from the tomogram, cut perpendicular to the z axis (the beam direction). This region contains three photoconverted structures whose connectivity with one another (at the point indicated by a *black X*) is difficult to determine. *x* and *y* show slices from the same volume, but taken perpendicular to the x and y axes, respectively. *X* marks the same spot in all three views. When analysis of structures from these three perspectives was still insufficient to reliably determine connectivity, other tools were employed. *z'* shows the same region as in *z*, one section deeper along the z axis, with a white line drawn to define a new orientation. *s* shows a slice of the tomogram in the orientation represented by the white line. In this view, the structures in question appear to be separate. On the computer screen, one can move the white line pixel by pixel, effectively serially sectioning the tomogram in any chosen orientation. We also used a modeling tool that let us extract and project 3-D information from a selection region. The extracted data could then be tumbled in space and rotated to any desired orientation. *t1*, *t2*, and *t3* show the volume around *X* in three orientations, confirming the inference made in *s*, that the structures in question are indeed distinct from one another.

were placed on ice, the medium removed, and the cells washed quickly two times with ice-cold HMEM. Cells were then incubated on ice with 5 nmol/ml ceramide/BSA complex in HMEM for 30 min. The ceramide solution was removed, and the cells washed twice with ice-cold HMEM and twice again with 37°C HMEM. The coverslips were then incubated at 37°C for 45 min, during which time some of the ceramide was metabolized by Golgi enzymes to BODIPY-sphingomyelin. A significant proportion of the probe remains as BODIPY-ceramide in the *trans*-Golgi network (Pagano et al., 1991). Cells were fixed with 2% glutaraldehyde in 0.1 M cacodylate, 5% sucrose, pH 7.2.

Photoconversion

After fixation, the cells were placed in 0.1 M Tris, 5% sucrose, pH 7.6, and observed with a Zeiss Universal fluorescence microscope to confirm proper intensity and localization of the BODIPY fluorescence (see corresponding figure in Pagano et al., 1991). Once confirmed, the coverslips were placed in a solution of 1.5 mg/ml DAB (Sigma Chem. Co.) in 0.1 M Tris–HCl, 5% sucrose, pH 7.6, and incubated for 10 min in the dark. The samples were then irradiated with an argon-ion laser (model 164; Spectra-Physics; λ_{ex} = 488 nm, power/area = 5 mW/mm^2) for ~15 min. The laser was equipped with a lens that expanded the beam to a diameter of 5 mm at the point of exposure, allowing several hundred cells to be irradiated at once. Following irradiation, a small brown spot could be observed, indicative of a DAB reaction. The DAB solution was removed and the cells were washed several times with 0.1 M Tris buffer. Photoconversion of the BODIPY fluorophore in the Golgi region was confirmed by phase-contrast microscopy using a 40× water-immersion lens (data not shown).

Electron Microscopy

Coverslips with adsorbed photoconverted cells were washed three times with 0.1 M cacodylate, 5% sucrose, pH 7.0, and then postfixed at room temperature with 2% OsO_4, 0.8% $K_3Fe(CN)_6$, 5% sucrose 0.1 M cacodylate for 15 min. Cells were washed several times with H_2O, dehydrated in a graded series of acetone-H_2O, and infiltrated with Epon-Araldite, and flat-embedded.

The embedded cell monolayer was observed by phase-contrast micros-

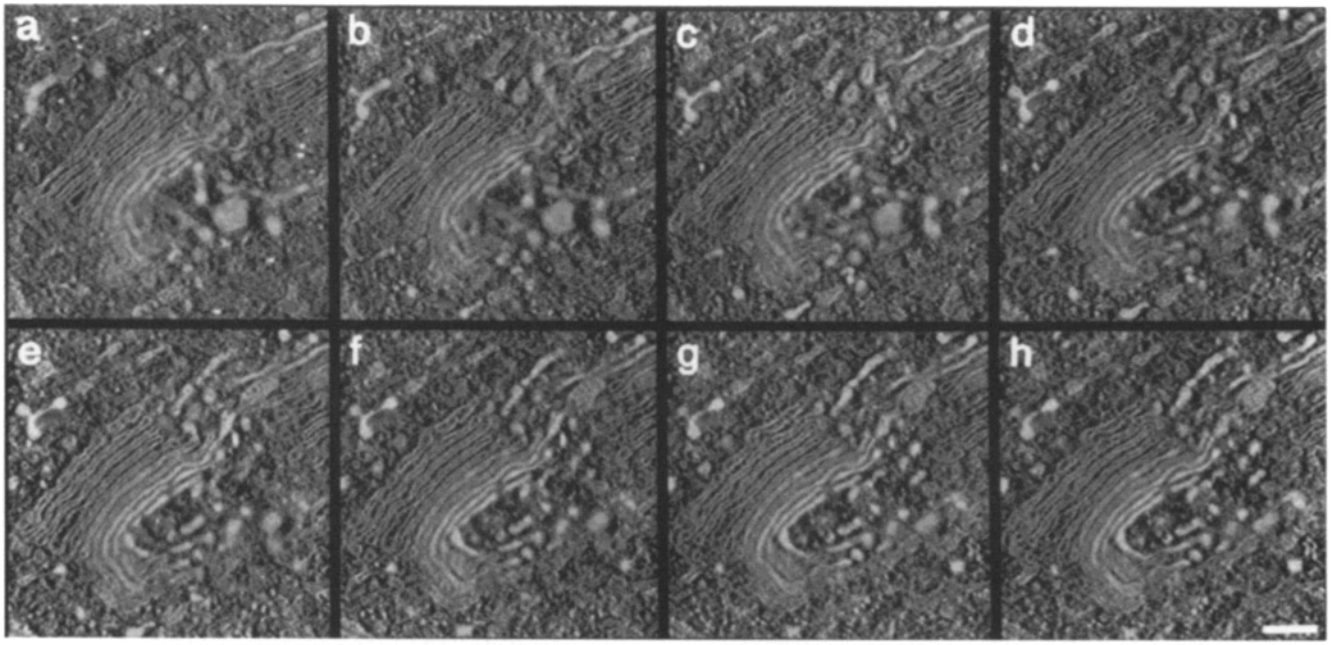

Figure 3. Eight 3.9-nm tomographic slices prepared from a 2° tilt-series. The photoconverted and ceramide-free cisternae are clearly distinguishable. Continuity among TGN elements can be appreciated as they are followed individually through the series (*a–h*). Note that multiple cisternae, in addition to TGN elements, are ceramide-positive, and that all such cisternae are continuous at their ends with TGN elements. The resolution of this reconstruction is ~10.3 nm.

copy and particular cells were chosen for remounting and sectioning. Thin sections (40 nm) were cut on a Reichert Ultracut-E ultramicrotome and viewed in a Philips CM-10 transmission electron microscope to confirm the exact localization of DAB reaction product within a Golgi complex and to determine the quality of structural preservation (data not shown).

High Voltage Electron Microscopy

Following selection of a suitable specimen, 250-nm sections were cut and placed on formvar-coated copper slot-grids. The sections were stained with 2% aqueous uranyl acetate and Reynold's lead citrate. Colloidal gold (10 or 15 nm) was applied to one surface of the grid to provide fiducial points for subsequent image alignment. Grids were carbon-coated on both sides to enhance their stability in the electron beam.

Specimens were placed in a tilt-rotate analytical stage (model 650; Gatan Inc., Pleasanton, CA) and viewed with a JEM-1000 HVEM operating at 1 MeV with a 30-μm objective aperture. Low magnification images of cells were taken to help identify well-preserved and well-stained Golgi complexes for high-resolution study (Fig. 1). Once selected, a Golgi region on a single 250-nm section was imaged near-focus at 18,300× and tilted ±60° with micrographs being taken at either 1- or 2°-intervals. Angular separation between views was measured with an optical encoder that displays the orientation of the specimen holder to within 0.1°. The specimen was irradiated before initiating the tilt series with ~15,000 e/Å^2 to limit anisotropic specimen thinning during data collection (Luther et al., 1988). Images were recorded on high-speed Kodak SO-163 film with a 2-s exposure at a dose rate of 9.1 e/Å^2 per second. Focusing was accomplished using a JEOL beam deflection system to examine an adjacent area along the tilt axis in order to limit the total electron dose to the area under study. Focus and specimen stability were confirmed using a fiber optically coupled TV system (model 622; Gatan, Inc.) equipped with an image intensifier. The nominal dose for each image in the tilt series was 90 e/Å^2.

Negatives were digitized with a cooled CCD camera (STAR-1; Photometrics, Ltd., Tuscon, AZ), using a pixel size that corresponded to 2.4 or 3.8 nm on the specimen. The transmitted light intensity was converted to optical density as previously described (Devaud et al., 1992). A computer program, TILTALIGN, was used to align the tilt series based on the known tilt angles and a model of the positions of the gold fiducial markers in each tilt view. A tomographic reconstruction was calculated from the aligned tilt series using the R-weighted back-projection algorithm (Gilbert, 1972; Wilson et al., 1992). Slices of the reconstructed volume were then cut and visualized either parallel or perpendicular to the beam. The resolution of the reconstructions was ~10 nm for the 2° series, and ~6 nm for the 1° series.

Production and analysis of tomographic reconstructions results in a reversal of image contrast. After comparing image clarity in such a view with the more conventional black-on-white display, we concluded that negative images were easier to interpret, thus in all figures that present tomographic data, images are in negative. Photoconverted product, as well as conventional EM stain, appear white. This distinguishes tomographic data from conventional electron micrographs, which are displayed in positive (see Fig. 1).

Tomographic data were viewed and analyzed with a Silicon Graphics R4000XZ graphics workstation using the model-rendering program, IMOD, developed in this laboratory, to facilitate reliable 3-D modeling from image data (see Fig. 7). In cases where it was difficult to determine if two TGN elements were connected or separate, special tools within the IMOD program were employed. These tools, illustrated in Fig. 2, allowed the tomographic data to be visualized in multiple orientations and perspectives to clearly define the borders of a particular structural element.

Results

The TGN varies significantly throughout a Golgi ribbon. Our major criteria for selecting particular regions for study were a minimal number of intruding organelles and an extensive TGN. We have produced seven tomographic reconstructions of TGN regions with resolutions of 6 or 10 nm. These show considerable variation in specific structure, such as the number of cisternae that stain with ceramide and the extent of the TGN. To display our findings we have selected two tomographic data sets that best illustrate some of the consistent structural features.

Multiple Cisternae are Labeled with Ceramide and Each of These Is Continuous with Elements of the TGN

Eight 3.9-nm slices from a tomographic reconstruction of a

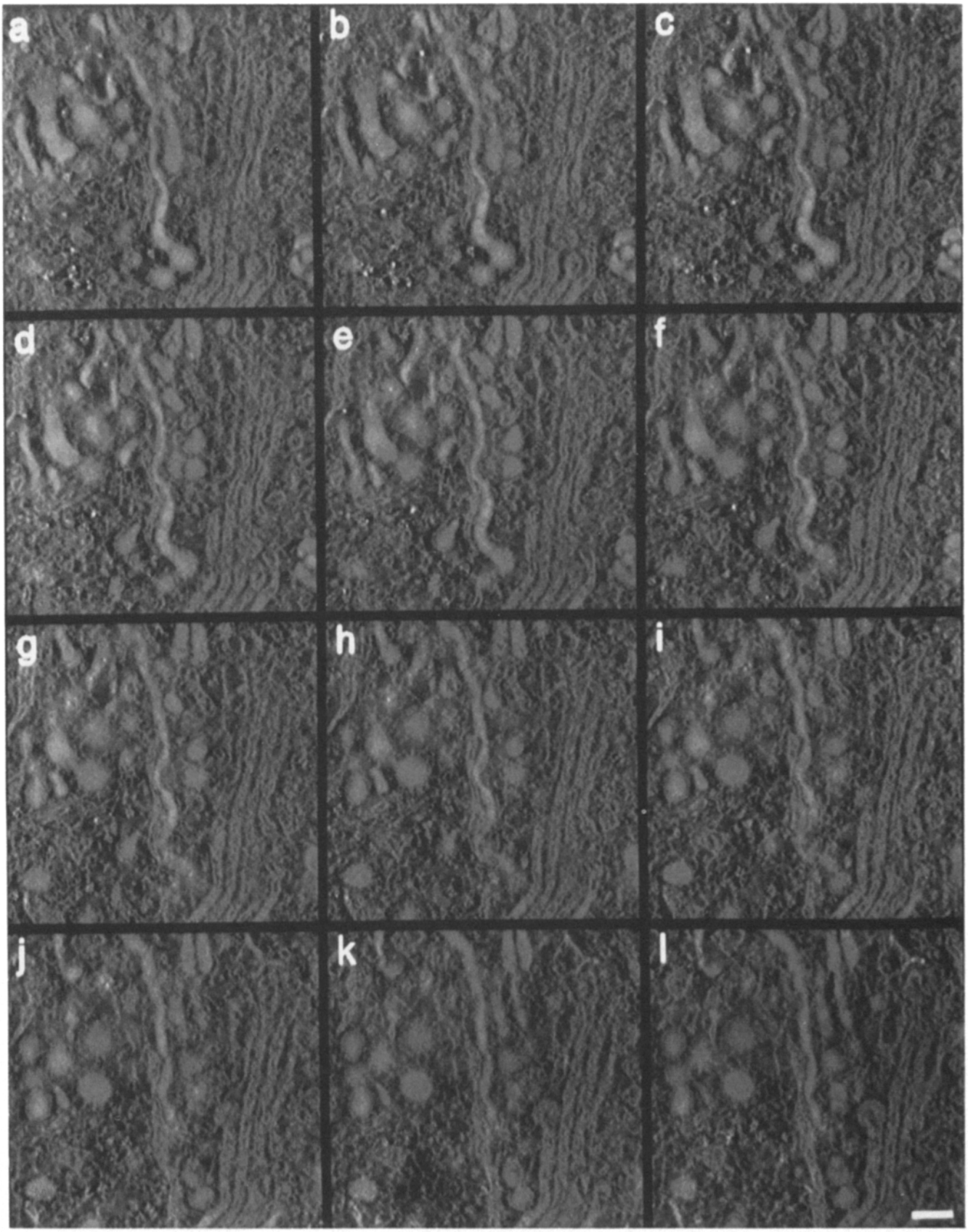

Figure 4. 12 sequential 2.4-nm tomographic slices prepared from a 1° tilt-series. Ceramide-positive TGN elements are clearly distinguishable from ceramide-free *cis* and *medial* cisternae. The tubularity of the TGN is obvious as individual elements are followed through the series (*a–l*). Note the presence of two distinct populations of vesicles associated with underlying tubules. The resolution of this data set is ~6 nm.

compact Golgi region adjacent to a noncompact region are shown in Fig. 3. The amount of photoconverted product increases in the *trans* direction. In this compact region, the three *trans*-most cisternae are strongly ceramide labeled. These cisternae remain parallel to the ceramide-free cisternae for some distance and then curve toward the TGN. This is an example of the "peeling off" phenomenon described by Rambourg (1979, 1990). In these peeled off regions, the ceramide-stained compartments lose their cisternal structure and are continuous with structures that comprise the TGN. Examination of the tomogram shows that the most heavily ceramide-labeled cisternae are continuous with tubules of the TGN, not just the *trans*-most cisterna. This feature of Golgi organization is displayed in the model shown in Fig. 7.

In a single tomographic slice, the TGN appears to be com-

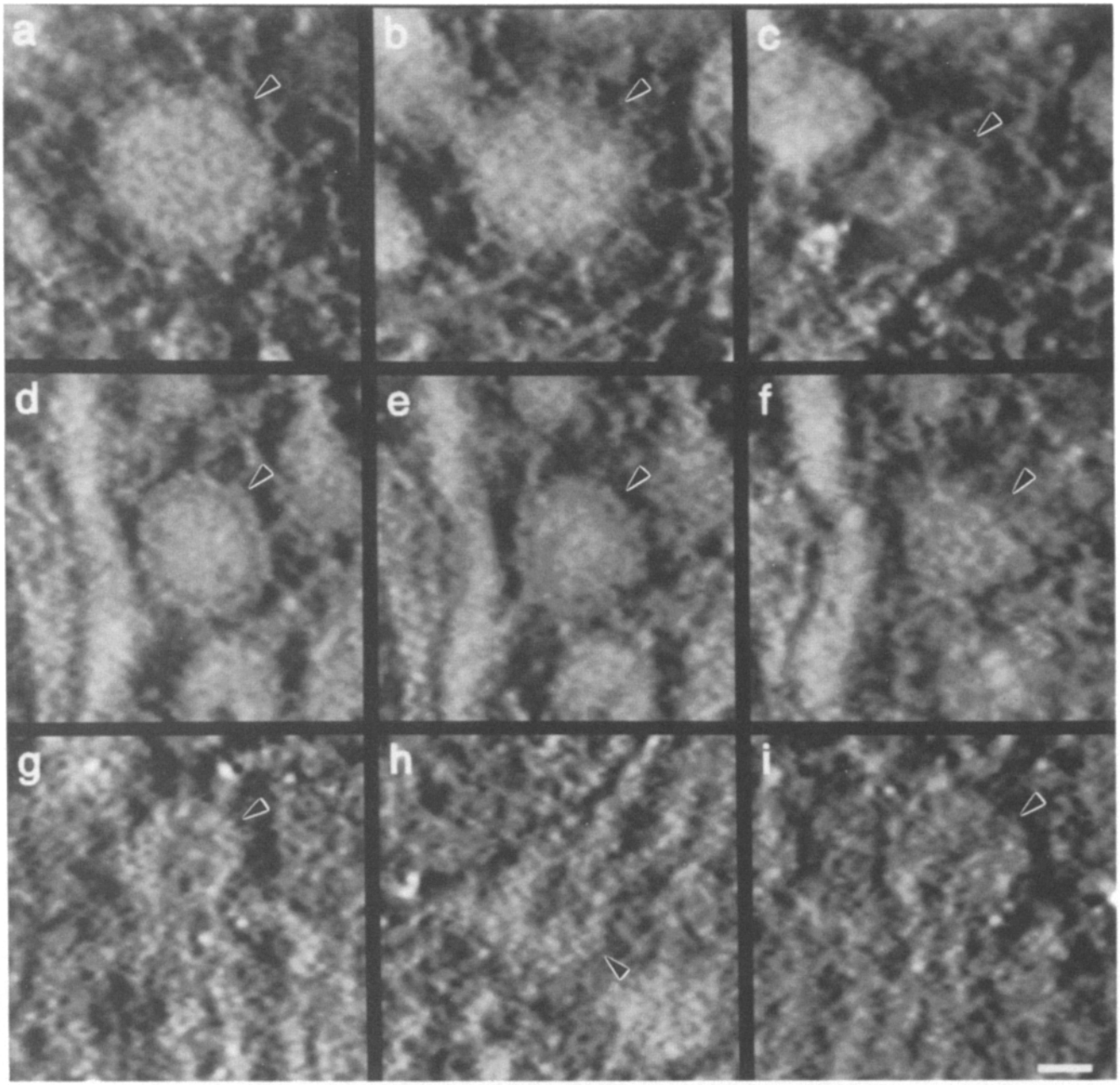

Figure 5. High-magnification comparison of two vesicle coat structures in the TGN. One vesicle population is identifiable as clathrin coated, on the basis of the spikes seen at the periphery in slices taken near the vesicle center (*a* and *b*), and the triskelion arms seen at the surface of such vesicles (*c*). Vesicles of the second population appear smaller than the clathrin vesicles and display a novel lace-like coat structure in images taken at their centers (*d* and *e*). Structures seen at the surface of these vesicles (*c*) are not comparable to similar views of the surface of clathrin vesicles. *g–i* show profiles of three coatomer-coated vesicles from the *cis* region of a Golgi stack (taken from a 1° tomographic reconstruction not shown in its entirety). Contrast of these structures is less than that of *trans* regions due to the absence of photoconvertion reaction product. The structure of the coat seen on these vesicles appears as a layer of small, packed particles. This structure is considerably different from both clathrin and the lace-like coat. Bar, 50 nm.

posed of individual vesicles of varying shapes and sizes. However, by moving through successive slices, it becomes evident that the TGN is composed of distinct tubules with little indication of anastomosis. The coat structures of vesicles are not discernible in this data set due to the resolution limit imposed by micrographs taken at only 2°-intervals. This tomogram is sufficient, however, to show a twist in the non-compact region that results in a reversal in the orientation of adjacent compact regions; the two TGNs displayed face in opposite directions. Note also the significant difference in the extent of the TGNs associated with these adjacent compact regions.

Two Distinct Types of Vesicles Originate from Different Elements of the TGN

Tomographic reconstructions calculated from a 1° tilt-series show improved 3-D resolution. 12 2.4-nm slices from such a reconstruction are shown in Fig. 4. Ceramide-positive cisternae are not visible in this display, but many elements of the TGN are clearly stained. The TGN is composed of multiple tubules that, in single slices, often appear as rows of vesicles. 3-D reconstruction demonstrates, however, that most of these vesicles are connected to a tubule, and are actually buds forming from a single element of the TGN.

The increased resolution of this reconstruction allows the coats of many budding profiles to be seen with improved clarity. Two distinct coat structures are visible on vesicles budding from TGN tubules: one has the lattice-like appearance of clathrin and the other has a novel lace-like structure. Coat structures are seen only on budding profiles, not on tubule surfaces. These two vesicle types always originate from distinct TGN tubules. Similar observations have been made in several 1° data sets, and our statement is based on a total of 71 vesicles whose coat morphology could be scored with confidence.

To gain more structural information about the novel lace-like coat, individual vesicles were selected and compared with clathrin-coated vesicles at the same magnification (Fig. 5). The clathrin vesicles (*a–c*) are ~100 nm in diameter, and the clathrin spikes are clearly visible in the tomographic slices that represent the middle portions of the vesicle (*a* and *b*). The contours of the clathrin triskelions come into view in slices cut near the edge of the vesicle (*c*).

Vesicles with the lace-like coat (Fig. 5, *d–f*) are ~60 nm in diameter. The coat structure is clearly visible in the tomographic slice from the mid-section of the vesicle (*d* and *e*). The term "lace-like" was selected to describe this coat, since it appears in these equatorial sections to be composed of scallop-shaped subunits with open spaces at their centers, separating the coat from the vesicle surface. In slices cut near the surface of the vesicle (*f*), the lace-like coat appears to be constructed from rectangular subunits that are often arranged at right angles to one another. They are packed together with a second smaller subunit to form the vesicle coat. The exact structure and arrangement of these subunits remain to be determined.

The structure of the lace-like coat is significantly different from the coatomer coat (Fig. 5, *g–i*). Tomographic slices taken from the midsections of vesicles budding individually from the ends of *cis* cisternae show a coat consisting of packed particles similar to that described by Weidman et al. (1993).

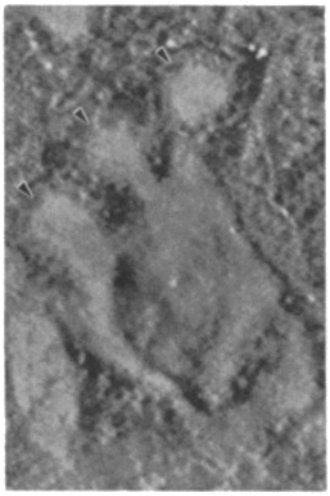

Figure 6. Tomographic slice (2.4 nm) showing synchronous budding of clathrin-coated vesicles from a single TGN tubule. The three budding profiles shown (*arrowheads*) are in slightly different orientations relative to the plane of the tomographic slice. The clathrin spikes are best visualized on the uppermost bud.

The formation of both clathrin and lace-like coated vesicles appears to be synchronous along a given tubule. We infer synchrony from the observation that all the vesicles associated with a given tubule are of approximately the same size. These structures are consistent with the idea that the formation of multiple vesicles on a TGN tubule starts at the same time and proceeds at the same rate. Whether the tubule is actually consumed in this process or a skeleton remains cannot be determined from these data.

The appearance of synchronous budding of TGN vesicles was observed in multiple data sets, and for both vesicle types. An example of synchronous budding of clathrin-coated vesicles, taken from a different data set, is shown in Fig. 6. Three clathrin vesicles are seen budding from a single TGN element. Other clathrin vesicles, projecting in different directions, are attached to this element in preceding sections (data not shown).

The TGN regions of these two data sets were modeled and projected as described in Methods. In these models (Fig. 7), color has been used to represent continuity between Golgi elements, and to distinguish between adjacent Golgi elements and between the two vesicle types. Several important features of Golgi structure are emphasized by these models, including the continuity of *trans*-cisternae with TGN elements, the tubular nature of the TGN, and the apparently synchronous budding of vesicles from TGN tubules. The finding that individual tubules produce vesicles on only one coat type is also clearly shown.

Discussion

This study provides new information on the 3-D structure of the *trans*-Golgi network and its relationship to the *trans*-cisternae. While several features of the TGN have been described by Rambourg and colleagues (reviewed in Rambourg and Clermont, 1990) and by others (Roth et al., 1985; Griffiths and Simons, 1986; Griffiths et al., 1989; Geuze and Morré, 1991), our 3-D reconstructions have put some earlier findings into a better context and also identified novel features of the Golgi complex: (*a*) multiple cisternal elements stain with photoconverted ceramide, and multiple ceramide-positive cisternae are continuous at their ends with photoconverted tubules of the TGN. Together, these results suggest that the compact region of the Golgi complex has several

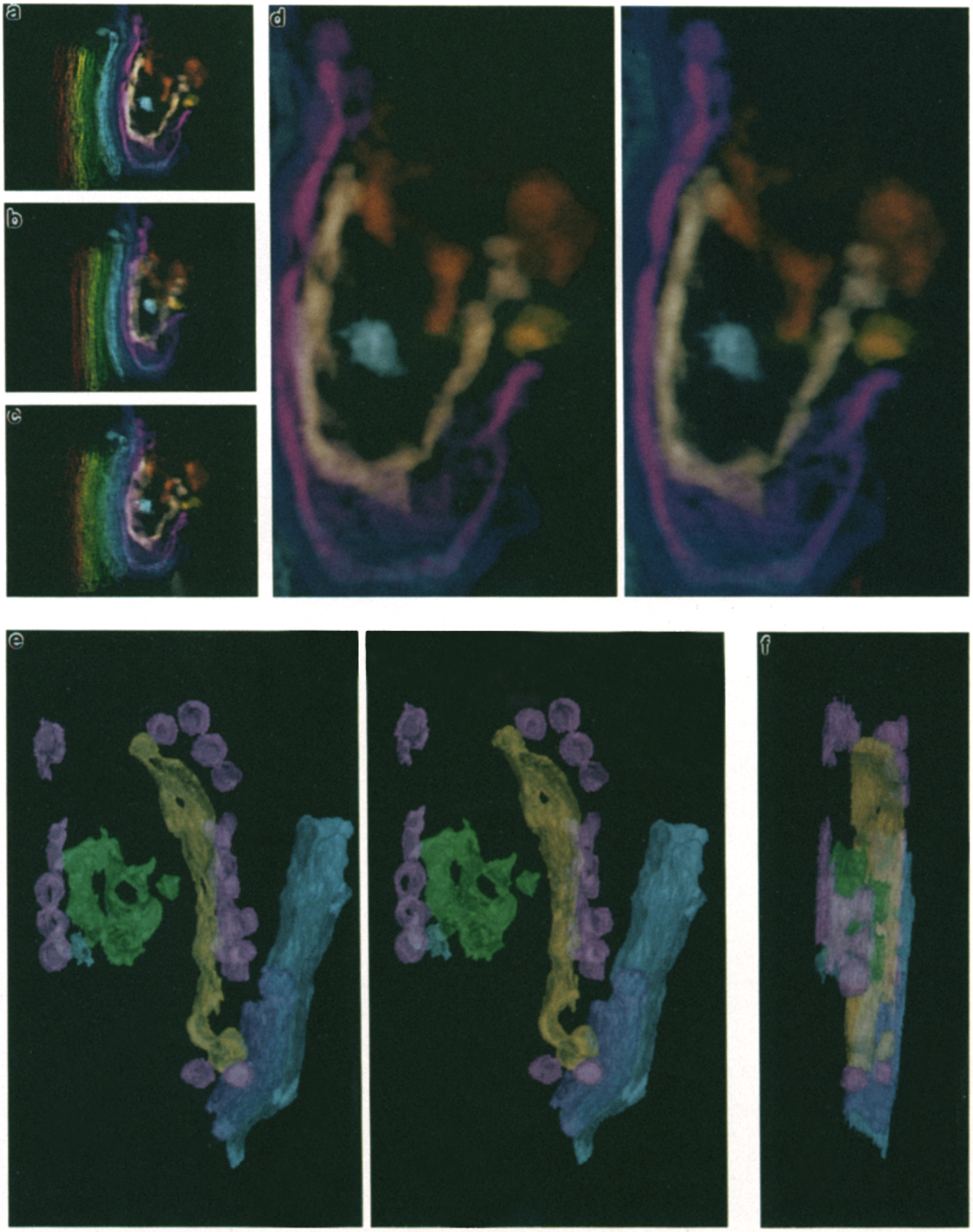

Figure 7. Models of Golgi tomograms. *a–d* show a model of most of the Golgi region from the tomogram in Fig. 3. The model was constructed by hand, using contours drawn on the membrane profiles visible in each slice of the tomogram. The image data from within each contour was extracted, added with comparable data from all other modeled slices and projected into a single 3-D representation. *a*, *b*, and *c* show projections oriented 0, +6, and −6°, respectively. Color is used to distinguish adjacent cisternae and elements of the TGN.

cisternae that can be defined as *trans*. (*b*) In single thin-section images or tomographic slices the TGN appears to be vesicular, but in 3-D the TGN is largely composed of distinct tubules; vesicular profiles emanate from and are usually continuous with individual tubules. There is little, if any, anastomosis between TGN tubules. (*c*) There are at least two morphologically distinct coats on the vesicles emanating from the TGN tubules: clathrin and a novel lace-like structure. Individual TGN tubules produce vesicles of only one coat type. (*d*) Vesicle formation appears to occur synchronously along the length of a tubule. This suggests that the tubule is consumed during the budding process. (*e*) Some regions of the Golgi ribbon have extensive TGN while others have minimal TGN. This is consistent with Rambourg's hypothesis that TGN elements are consumed during vesicle budding (Rambourg et al., 1979). These morphological findings have profound implications on our concepts of the mechanisms by which proteins and lipids are sorted into vesicles for delivery to post-TGN locations.

Our images of continuity between ceramide-positive TGN elements and multiple ceramide-positive cisternae are consistent with the observations of Rambourg et al. (1979), that in regulated secretory cells, condensing vacuoles appear to form from several *trans*-cisternae. Continuity of only ceramide-positive cisternae with TGN elements is further evidence that these cisternae are trans. Our images are also in agreement with Griffiths et al. (1989), in showing that the TGN is continuous with the ends of *trans*-cisternae, rather than with multiple points in the middle of the single, *trans*-most cisterna.

In our reconstructions the TGN is tubular, and almost all vesicular profiles seen in single tomographic slices are connected with tubular components when visualized in 3-D. Vesicles not associated with tubules are few in number and are distributed throughout the TGN region. We have found no evidence for anastomosis of TGN tubules or the vesicles emanating from them. This is in contrast to published thin-section images (see Fig. 5 *b*, Griffiths et al., 1985; Fig. 1, Geuze and Morré, 1991).

There are two major populations of vesicles that bud from the TGN in constitutively secreting nonpolarized cells, such as the NRK. One, which is clathrin-coated, carries newly synthesized lysosomal proteins via the mannose-6-phosphate receptor to the endocytic-lysosomal pathway (Kornfeld et al., 1989). The second population carries newly synthesized molecules to the plasma membrane. These vesicles are not clathrin coated (Griffiths et al., 1985) but no distinct coat structure has been visualized on them. While it is generally assumed that a coat is essential to deform the membrane and drive the budding process (see Melançon et al., 1991), only two coat structures have been described: clathrin and coatomer (Orci et al., 1986). Evidence suggests that coatomer-coated vesicles are not present in the TGN. The coatomer protein, β-COP (Duden et al., 1991), has been localized predominantly in *cis*-Golgi (Oprins et al., 1993). β-COP has been shown to function in ER to Golgi transport, both in vitro (Peter et al., 1993) and in vivo (Pepperkok et al., 1993), and it has no apparent function in transport from the TGN to the plasma membrane (Pepperkok et al., 1993).

Using 3-D tomographic reconstruction we have visualized a new coat structure on buds and vesicles emanating from TGN tubules. This coat appears lace-like; the edges are scalloped and the center of each scallop appears hollow, as if cut out. Buds displaying this coat are smaller in diameter (~60 nm) than clathrin-coated buds (~100 nm) in the same region. The structural proteins of the lace-like coat may not yet be biochemically defined, but the morphological characterization of the coat will certainly motivate a molecular identification of the constituent proteins.

In our images, clathrin and lace-like coated vesicles often appear as rows of buds emanating from TGN tubules; one tubule produces clathrin-coated buds and another produces lace-like–coated buds. Individual tubules do not produce buds of both types. These observations have three implications: (*a*) there are multiple steps in the process of vesicle formation. The row of buds image (Fig. 4) may represent an intermediate step that is awaiting a signal for the buds to dissociate and become free vesicles; (*b*) given the relative volume of a TGN tubule and the sum of all vesicles connected with it, tubules may be consumed in the process of vesicle formation; (*c*) sorting of molecules must occur prior to the formation of TGN tubules.

The concept that molecules have already been sorted in the TGN was suggested by Geuze et al. (1987, 1988), who showed that receptors are not uniformly distributed in the membranes of the TGN in rat hepatocytes. Double immunogold labeling experiments, in which asialoglycoprotein and mannose-6-phosphate receptors, which are destined to the plasma membrane and the endocytic pathway respectively, were localized to distinct regions of the TGN. However, these experiments were carried out on single thin cryosections, and so could not reveal 3-D spatial information about the compartments containing the different receptors. The information presented here predicts that immunolocal-

The dark blue, magenta, and pink cisternae peel away from the other cisternae and are continuous with TGN tubules. These are the elements which are most heavily photoconverted (see Fig. 4). The light blue structure in the center of the TGN is a large, free vesicle. *d* is a stereo-pair detail of the trans cisternae and elements of the TGN, which clearly displays the tubular nature of the TGN and lack of anastamosis between adjacent elements. *e* and *f* depict a model of the tomogram in Fig. 4. This model is a display of the surfaces of the contours rather than a projection of their content. The cisternae on the right, shown in blue and purple, are *trans*-Golgi cisternae, and all other features of the model are elements of the TGN. Connections between the *trans* cisternae and TGN are not visible in this data set. Color is used to distinguish the two different coat morphologies; magenta represents lace-like coated buds and associated tubules, and green represents clathrin coated buds and associated tubules. The proximal magenta element is producing at least 11 lace-like vesicles. The distal one is producing at least three. A fourth lace-like vesicle, in the upper left, is likely to be connected with the distal tubule, but the connecting element is not within the plane of original 250-nm plastic section. The yellow tubule appears to be producing lace-like buds from its ends. The small blue object separating the green clathrin element from the distal lace-like element is a portion of a TGN tubule, seen in cross-section, most of which is not present in the plane of the section. *e* is a stereo pair that demonstrates the 3-D positions of all components. *f* is an edge view that clearly shows the tubular connections between several lace-like vesicles (*magenta*) that appear distinct in other views (see *e*).

ization studies will demonstrate homogeneous labeling of entire TGN tubules; some tubules will contain molecules destined for the plasma membrane, while others will contain molecules destined for the endocytic pathway. Our observations indicate that sorting of molecules occurs before the formation of TGN tubules, most likely upon delivery to the *trans*-cisternae. This hypothesis is inconsistent with widely held models for Golgi function, which state that sorting events take place within the TGN (Griffiths and Simons, 1986; Geuze and Morré, 1991; Mellman and Simons, 1992).

Several molecules have been identified that are candidates for structural components of the lace-like coat. One is a cytoplasmic complex that consists of a 62-kD protein (p62) and three low molecular weight GTPases, one of which is rab6. This complex must associate with a TGN integral membrane protein, TGN38/41, for the budding of exocytic vesicles to occur. It remains present on vesicles destined for the plasma membrane (Jones et al., 1993). Another candidate is the coat-like protein, p200, described by Narula et al. (1992), which is localized primarily in the TGN (J. Stow, personal communication). Neither frozen nor standard, plastic-embedded thin sections have allowed coat structures to be visualized on plasma membrane-bound vesicles (Griffiths et al., 1985) or on those known to be associated with the p62 complex (Howell et al., 1994). In both cases, however, clathrin-coated profiles can be seen in the TGN. Immunolabeling studies with resolution approximating that of our tomographic reconstructions will be required to determine if the p62 complex, p200, or other molecules form the lace-like coat structure.

The studies reported in this paper have focused on selected regions of the TGN in NRK cells. Future experiments will need to focus on regions of the Golgi ribbon not analyzed for these studies; most importantly noncompact regions and areas containing minimal TGN. Additional features will be revealed when the TGN is studied in different functional states and in other cell types.

We thank Richard Pagano for his help in establishing the photoconversion technique, and David Mastronarde for use of the TILTALIGN program.

This work was supported by National Institutes of Health Biotechnology Resources grant RR00592 to J. R. McIntosh, and National Institutes of Health grant GM42629 to E. Howell.

Received for publication 24 May 1994 and in revised form 7 July 1994.

References

Cooper, M. S., A. H. Cornell-Bell, A. Chernjavsky, J. W. Dani, and S. J. Smith. 1990. Tubulovesicular processes emerge from trans-Golgi cisternae, extend along microtubules and interlink adjacent trans-Golgi elements into a reticulum. *Cell.* 61:135–145.

Devaud, G., P. S. Furcinitti, J. C. Fleming, M. K. Lyon, and K. Douglas. 1992. Direct observation of defect structure of protein crystals by atomic force and transmission electron microscopy. *Biophys. J.* 63:630–638.

Duden, R., G. Griffiths, R. Frank, P. Argos, and T. E. Kreis. 1991. β-COP, a 110 kd protein associated with non-clathrin-coated vesicles and the Golgi complex, shows homology to β-adaptin. *Cell.* 64:649–665.

Farquhar, M. G., and G. E. Palade. 1981. The Golgi apparatus (complex)-1954-1981- from artifact to center stage. *J. Cell Biol.* 91:77s–106s.

Geuze, H. J., J. W. Slot, and A. L. Schwartz. 1987. Membranes of sorting organelles display lateral heterogeneity in receptor distribution. *J. Cell Biol.* 104:1715–1723.

Geuze, H. J., W. Stoorvogel, G. J. Strous, J. W. Slot, J. E. Bleekemolen, and I. Mellman. 1988. Sorting of mannose 6-phosphate receptors and lysosomal membrane proteins in endocytic vesicles. *J. Cell Biol.* 107:2491–2501.

Geuze, H. J., and D. J. Morré. 1991. Trans-Golgi reticulum. *J. Electron Microsc. Tech.* 17:24–34.

Gilbert, P. F. C. 1972. The reconstruction of a three-dimensional structure from projections and its application to electron microscopy. II. Direct methods. *Proc. R. Soc. London B Ser. Biol. Sci.* 182:89–102.

Griffiths, G., S. Pfeiffer, K. Simons, and K. Matlin. 1985. Exit of newly synthesized membrane proteins from the *trans* cisternae of the Golgi complex to the plasma membrane. *J. Cell Biol.* 101:949–964.

Griffiths, G., and K. Simons. 1986. The trans-Golgi network: sorting at the exit site of the Golgi complex. *Science (Wash. DC).* 234:438–443.

Griffiths, G., S. D. Fuller, R. Back, M. Hollinshead, S. Pfeiffer, and K. Simons. 1989. The dynamic nature of the Golgi complex. *J. Cell Biol.* 108:277–297.

Hong, W., and B. L. Tang. 1993. Protein trafficking along the exocytotic pathway. *Bioessays.* 15:231–238.

Howell, K. E., J. R. Crosby, M. S. Ladinsky, S. M. Jones, R. Schmid, and J. Ugelstad. 1994. Magnetic solid supports for cell-free analysis of vesicular transport. *In* Advances in Biomagnetic Separation. M. Uhlén, E. Hornes, and Ø. Olsvik, editors. Eaton Publishing Co., Natick, MA. 195–204.

Jones, S. M., J. R. Crosby, J. Salamero, and K. E. Howell. 1993. A cytosolic complex of p62 and rab6 associates with TGN38/41 and is involved in budding of exocytic vesicles from the *trans*-Golgi network. *J. Cell Biol.* 122:775–788.

Kornfeld, S., and I. Mellman. 1989. The biogenesis of lysosomes. *Annu. Rev. Cell Biol.* 5:483–525.

Luther, P. K., M. C. Lawrence, and R. A. Crowther. 1988. A method for monitoring the collapse of plastic sections as a function of electron dose. *Ultramicroscopy.* 24:7–18.

Melançon, P., A. Franzusoff, and K. E. Howell. 1991. Vesicle budding: insights from cell-free assays. *Trends Cell Biol.* 1:165–171.

Mellman, I., and K. Simons. 1992. The Golgi complex: in vitro veritas. *Cell.* 68:829–840.

Narula, N., I. McMorrow, G. Plopper, J. Doherty, K. S. Matlin, B. Burke, and J. L. Stow. 1992. Identification of a 200-kD, brefeldin-sensitive protein on Golgi membranes. *J. Cell Biol.* 117:27–38.

Oprins, A., R. Duden, T. E. Kreis, H. J. Geuze, and J. W. Slot. 1993. β-COP localizes mainly to the *cis*-Golgi side in exocrine pancreas. *J. Cell Biol.* 121:49–59.

Orci, L., B. S. Glick, and J. E. Rothman. 1986. A new type of coated vesicle carrier that appears not to contain clathrin: its possible role in protein transport within the Golgi stack. *Cell.* 46:171–184.

Pagano, R. E., M. A. Sepanski, and O. C. Martin. 1989. Molecular trapping of a fluorescent ceramide analogue at the Golgi apparatus of fixed cells: interaction with endogenous lipids provides a *trans*-Golgi marker for both light and electron microscopy. *J. Cell Biol.* 109:2067–2079.

Pagano, R. E., O. C. Martin, H. C. Kang, and R. P. Haugland. 1991. A novel fluorescent ceramide analogue for studying membrane traffic in animal cells: accumulation at the Golgi apparatus results in altered spectral properties of the sphingolipid precursor. *J. Cell Biol.* 113:1267–1279.

Pepperkok, R., J. Scheel, H. Horstmann, H. P. Hauri, G. Griffiths, and T. E. Kreis. 1993. β-COP is essential for biosynthetic membrane transport from the endoplasmic reticulum to the Golgi complex in vivo. *Cell.* 74:71–82.

Peter, F., H. Plutner, H. Zhu, T. E. Kreis, and W. E. Balch. 1993. β-COP is essential for transport of protein from the endoplasmic reticulum to the Golgi in vitro. *J. Cell Biol.* 122:1155–1167.

Rambourg, A., and Y. Clermont. 1990. Three-dimensional electron microscopy; structure of the Golgi apparatus. *Eur. J. Cell Biol.* 51:189–200.

Rambourg, A., Y. Clermont, and L. Hermo. 1979. Three-dimensional architecture of the Golgi apparatus in Sertoli cells of the rat. *Am. J. Anat.* 154:455–476.

Roth, J., D. J. Taatjes, J. M. Lucocq, J. Weinstein, and J. C. Paulson. 1985. Demonstration of an extensive trans-tubular network continuous with the Golgi apparatus stack that may function in glycosylation. *Cell.* 43:287–295.

Rothman, J., and L. Orci. 1992. Molecular dissection of the secretory pathway. *Nature (Lond.).* 355:409–415.

Takazawa, P. A., J. K. Yucel, B. Veit, D. J. Faulkner, T. Deerinck, G. Soto, M. Ellisman, and V. Malhotra. 1993. Complete vesiculation of Golgi membranes and inhibition of protein transport by a novel sea sponge metabolite, Ilimaquinone. *Cell.* 73:1079–1090.

Weidman, P., R. Roth, and J. Heuser. 1993. Golgi membrane dynamics imaged by freeze-etch electron microscopy: views of different membrane coatings involved in tubulation versus vesiculation. *Cell.* 75:123–133.

Wilson, C. J., D. N. Mastronarde, B. McEwen, and J. Frank. 1992. Measurement of neuronal surface area using high-voltage electron microscope tomography. *Neuroimage.* 1:11–22.